Hovering Microswimmers Exhibit Ultrafast Motion to Navigate under Acoustic Forces

Jean-François Louf, Nicolas A Bertin, Benjamin Dollet, Olivier Stéphan, Philippe Marmottant

PREPRINT

Advanced Materials Interfaces

Hovering Microswimmers Exhibit Ultra-Fast Motion to Navigate under Acoustic Forces

Jean-François Louf[1] | Nicolas Bertin[1] | Benjamin Dollet[1] | Olivier Stephan[1] | Philippe Marmottant[1]

[1]University Grenoble Alpes and CNRS, UMR 5588 LiPhy, Saint-Martin-d'Hères, 38402, France

Correspondence
Jean-François Louf, University Grenoble Alpes and CNRS, UMR 5588 LIPhy, Saint-Martin-d'Hères, 38402, France
Email: jeanfrancois.louf@gmail.com

Funding information
This work was supported by the European Research Council (ERC) under the European Union Horizon 2020 Research and Innovation programme (grant agreement No 614655 "Bubbleboost").

The goal of this study is to engineer 3D-microswimmers containing a bubble that can be stimulated and guided with acoustic waves emitted by transducers. By using 3D-microfabrication techniques, we designed 20×20×26 μm swimmers with a trapped air bubble pointing towards the substrate, thus mimicking an hovercraft. We then remotely applied acoustic vibrations to the bubble, which generates a strong steady flow (0.1-2 mm/s), an effect referred as acoustic streaming, resulting in a jet below the hovercraft. We found that the motion of the swimmer relies on two parameters, namely the frequency and amplitude of the acoustic wave. We measured the swimmer velocities and observed a very wide distribution: from 0.05 to 350 mm/s or 17500 body lengths. Such a high velocity in terms of body length makes this swimmer one of the fastest among the different microswimmers reported in the literature.[1] The motion of the swimmer is found to be a combination of two forces orientated in different directions: the streaming force and the radiation force. While the first one is reducing adhesion, the second one is helping the motion. Using different transducers orientated towards different directions, we were able to navigate the swimmer into different directions as well.

KEYWORDS
acoustic streaming, microswimmers, radiation force

1 | INTRODUCTION

These last decades have witnessed the emergence of many new techniques and ideas in microfluidics. Among them, microswimmers are of particular interest.[1–6] Being able to move at such low Reynolds number is very challenging, but scientists have come with numerous ways to overcome that issue. As a result, different "motors" exist. For example, among the most populars ones, one can find phoretic microswimmers[7–14] that often use asymmetric chemical gradients to move, or magnetic ones[15–19] that can be controlled from afar and do not involve the potentially toxic chemical reactions commonly used to propel phoretic swimmers.[20] Other interesting locomotion techniques, are by using bubbles production[21,22] or acoustic vibrations[23–25] to propel the objects. Due to its wide utilization in medical applications, acoustic energy is a very interesting candidate as a driving mechanism. However, research in this area have so far been limited to 2D soft microswimmers.[23,24] In this configuration it is hard to change the direction of motion or to control it accurately.

Recently, advances in microfabrication have enable researchers to trap bubbles in very well defined tiny objects. Using microphotolithography, Feng *et al.* have been able to trap a 60 μm diameter bubble into a tiny cylinder, and by applying acoustic waves, they generated a periodic oscillation of the gaseous bubble that induces motion of this cylinder.[26] Such microswimmers present a lot of interest, as they are easy to make, small enough to navigate into blood vessels, and the motor does not produce any waste (chemicals); however, the maneuverability, range of motion and accuracy may not be optimal. Recently, the same authors were able to address these issues by making other 2D-microswimmers using microstreaming forces from different bubble oscillation at different resonances ~~radiation forces~~ to move. The bubble oscillations ~~radiation forces~~ were induced by making the water tank to vibrate using piezoelectric transducers.[27] Another microfabrication technique, this time using two-photon absorption microscopy, have recently been investigated to make microobjects encapsulating bubbles.[28] In their work, Bertin *et al.*[28] have been able to build these 10 μm diameter capsules with an accuracy of 1 μm. This technique is very enticing, and we chose to use these capsules as "motors" for our microswimmers.

The main goal of this study is to be able to move the 3D-fabricated objects and to control their motion using an actuator from afar without inducing vibration of the tank, for the long term goal of drug delivery in the human body. But to do so, many questions have to be solved before: How to overcome adhesion between the microswimmer and the substrate? What controls the direction of motion? What are the forces involved? And what is the best design?

In this study we built 3D microswimmers using two-photon absorption microscopy techniques, see Figure 1. A gas bubble pointing downwards is trapped into each of them, and by applying acoustic waves (250-450kHz), we were able to hover the objects over the substrate and to induce their motion. The theoretical motion dynamics and the forces involved are investigated in section 2 of the article. In section 3 we present our results obtained by varying the different key parameters: the frequency and the amplitude of the acoustic waves. We continue on section 4 with a discussion on the motion of the swimmer and the forces involved, and in section 5 with a conclusion of our results. We end in section 6 by describing the fabrication process and the set-up apparatus.

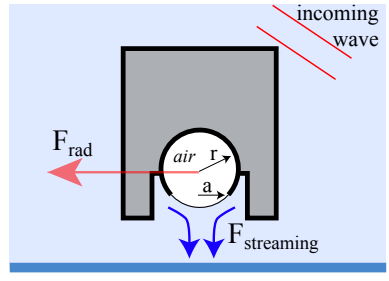

FIGURE 1 Principle of a hovering microswimmers, 3D fabricated to contain a bubble (of radius *r*), with an open interface below (of half-width *a*). The free interface is able to vibrate generating a streaming jet below.

2 | BUBBLE-BASED SWIMMERS: THEORY, RADIATION AND STREAMING FORCES

Under acoustic waves, the gas pocket contained in the microswimmer pulsates, with an amplitude ϵr, r being the radius of the spherical shell surrounding the bubble. This gives rise to two different effects: (i) a radiation force exerted by the incoming acoustic waves, (ii) a streaming jet emitted away from the pulsating interface, see Figure 1.

The radiation force is given by $F_{\text{rad}} = -\langle \Delta V(t) \nabla p(t) \rangle$ where $\Delta V(t)$ is the variation of the gas volume when the interface vibrates. We can evaluate this force using the fact that $\Delta V(t)$ scales like ϵr^3, while the pressure gradient scales like the applied pressure amplitude P_{ac} divided by the wavelength $\lambda = c_l/f$, f being the frequency and c_l the speed of sound in water. As a result the radiation force scales like $F_{\text{rad}} \sim \epsilon r^3 P_{ac} f / c_l$.

The streaming force generated by the streaming is a nonlinear effect, and it writes $F_{\text{streaming}} \sim \epsilon^2 \rho_l r^4 f^2$ according to Ref.[28]

The vibration amplitude is a function of frequency $\epsilon(f)$ and exhibits a resonance. If we simplify the vibration dynamics by considering that the bubble is a spherical harmonic oscillator obeying the Rayleigh-Plesset equation,[29] the amplitude of vibration writes for small pressures $\epsilon(f) = \epsilon_0 / \sqrt{(1 - f^2/f_0^2)^2 + (f/f_0 Q)^2}$, with $\epsilon_0 = P_{ac}/4\pi^2 \rho_l r^2 f_0^2$, where f_0 is the resonance frequency, and Q the quality factor of the resonance. For a bubble of size $r = 10\,\mu$m, resonating at $f_0 = 320$ kHz, an acoustic pressure of $P_{ac} = 1$ kPa (as in Ref.[28]), we have $\epsilon_0 = 2.5 \times 10^{-3}$. At resonance, $\epsilon(f_0) = \epsilon_0 Q$, where the quality factor Q is of order of a few units.[29] Hence ϵ remains much smaller than 1, which justifies the use of a harmonic oscillator model.

The streaming force to radiation force ratio is therefore $F_{\text{streaming}}/F_{\text{rad}} = \epsilon \rho_l r f c_l / P_{ac}$, and for the typical aforementioned values, this ratio is of order 10. This means the propulsion by streaming is preponderant. However, here, the streaming jet is directed towards the substrate boundaries, ensuring a repulsion, and avoiding to stick to the bottom surface. The radiation forces applied by the transducer then induce a lateral motion.

3 | RESULTS

3.1 | Streaming velocity from the propelling bubble

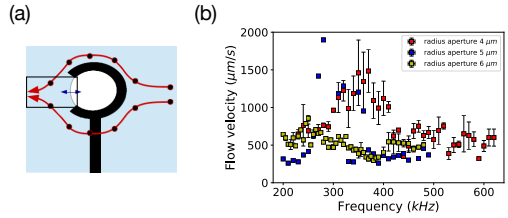

FIGURE 2 (a) Schematic of the experiment measuring the flow of the streaming jet generated by a vibrating bubble, here placed horizontally and attached to the substrate. The black rectangle indicates the area where the flow velocity is measured. (b) Experimental flow velocity behind AMBs of three different aperture radii: 4, 5 and 6 μm. The error bars come from the average of the flow velocity behind two AMB.

To test the performance of the propelling jets produced by the bubble vibration we studied specifically bubble enclosed in an open shell. For the purpose of this study it is fabricated on a pillar attached to the substrate, and oriented horizontally, introduced in Bertin et al. [28] under the name armored microbubbles (AMB). We tested different aperture diameters: 4, 5 and 6 μm (see Figure 2(a)). The flow velocity behind each AMB is measured using a combination of a PIV software,[30] and a homemade Python code. Figure 2(b) shows the flow velocity behind each AMB for different frequencies. We can see that for each radius aperture, a maximal flow velocity is reached at a specific frequency, different from the peak frequency of the transducer (200 kHz here): the resonance frequency of the AMB. We experimentally find resonance frequencies of 360kHz, 280kHz, and 250kHz, for respectively AMBs of aperture radii of 4μm, 5μm, and 6μm. In the model from Bertin et al. [28], the same AMBs have predicted resonance frequencies of respectively 470kHz, 330kHz, and 250kHz. The measured resonance frequencies and the predicted ones from the model seem to converge when the aperture radii are increasing. In particular, we highlight that for the AMB of 4 μm radius aperture, a resonance frequency of 360 kHz is experimentally measured. This AMB is of

particular interest as it will be used as the motor of our micro-swimmers later on.

3.2 | Micro-swimmers characterization

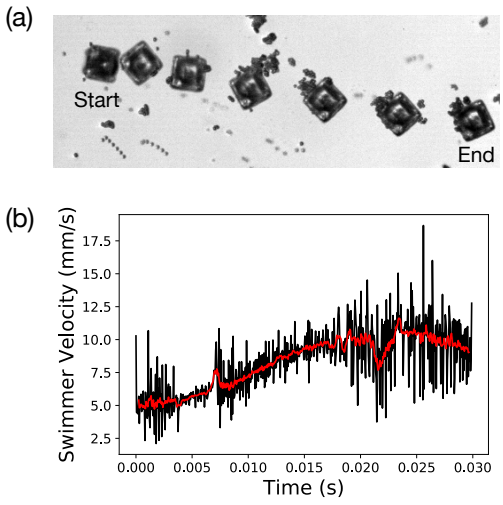

FIGURE 3 Trajectory and velocity of a swimmer excited at 360 kHz. (a) Trajectory of the swimmer shown with the superposition of several images. (b) Velocity profile of the swimmer. The black line indicates the raw data, while the red line is a moving average over 5 points. The maximal value of the red line is our control parameter.

We now use our experimental set-up to induce propagative acoustic waves on our microswimmers to investigate their motion response with the transducer peaked at 350 kHz. We vary the frequency as well as the amplitude of the signal which are easily tunable parameters. The design of the microswimmers, with the bubble pointing downwards, allows the acoustic streaming to induce the hovering of the swimmers, thus overcoming any problem of adhesion. Combined with the radiation force resulting from the acoustic wave, a clear motion of the swimmers is observed. Using an adapted particle tracking code from Trackpy[31] we are able to easily follow the position of the center of mass of the swimmers. A typical trajectory can be seen in Figure 3(a). The velocity profile can be extracted from the position profile (see Figure 3(b)). We use a gliding average on 5 points to smooth the data and we define the maximal velocity as our measurement. That velocity reaches a peak value near 370 kHz. At that frequency, our 20 μm swimmer is able to reach ultra fast velocities up to 0.35 m/s, or 17500 body lengths. Interestingly, that maximal velocity of the swimmer is reached close to the resonance frequency of the AMB (360 kHz). Other experiments run with the transducer peaked 200 kHz show the same resonance frequency (360 kHz) but with smaller velocities (0.05-15 mm/s). This reduce maximal velocity is due to the mismatch between the resonance frequency of the swimmer and the transducer peaked at 200 kHz.

We also varied the amplitude of the acoustic waves from 5 kPa to 24 kPa (Figure 4(b)), which was measured using a calibrated needle hydrophone. As the amplitude increases, the velocity increases as well. Data are compatible with a quadratic increase, although with significant scatter; this agrees with our theoretical discussion of the acoustic driving forces, being a nonlinear effect.

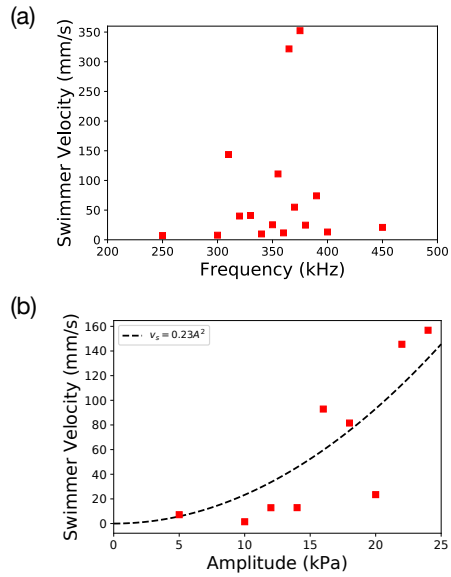

FIGURE 4 (a) Maximal mean velocity as a function of the acoustic wave frequency. We can see a noticeable peak at frequencies between 360 kHz and 380 kHz. (b) Maximal mean velocity as a function of the amplitude of the acoustic wave at a frequency of 250 kHz. The dashed line is a quadratic fit of the data.

3.3 | Micro-swimmers maneuverability

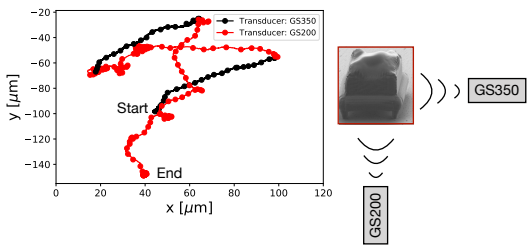

FIGURE 5 Trajectory of a swimmer under the successive influence of two transducers orientated perpendicularly to each other. The frequency of excitation of both transducers is 300 kHz, and their amplitudes are the following: GS200: 200 mVpp, GS350: 80 mVpp.

Once the micro-swimmers motion is characterized, it is now possible to play with the direction of motion. As we saw in section 2, depending on the transducer's location, the swimmer motion will be in a specific direction. Subsequently, by putting different transducers pointing in different directions, it is possible to orientate the motion of the swimmers. We performed such experiment by playing with the transducers actuation. In Figure 5, two transducers oriented perpendicularly are set-up and then activated alternatively. Firstly the transducer GS350 is activated, and the swimmer goes toward it (in black). It is then tuned off, and the second transducer is activated (GS200), inducing a displacement of the swimmer to the left (in red). We then repeated the same procedure again.

4 | DISCUSSION

These results can be further investigated by looking at the motion direction properties. Indeed, we apply a propagative wave that induces a radiation force on the bubble contained in the swimmers. The resulting motion from this force is to be compared with the force acting on the swimmers resulting from the vibration of the air bubble (acoustic streaming) under them. But when we look at the motion of the micro-swimmers, we observe different behaviors. First, it can either go along a straight line, or curl (Figure 6). This is due to the direction of the streaming force. If that force is perpendicular to the substrate it will just hover the swimmers, but if while the swimmers are getting unhooked, somehow they are a bit tilted, then this force will induce a rotation of the swimmers. Second, the sense of motion is not constant. When applying a propagative wave, we would expect the swimmers to be always pushed away from the transducer. However, as seen in Fig.5, the sense of motion is not strictly given by the wave direction. Explanations on this behavior remain elusive and further experiments are needed to have a clear answer, but the presence of standing acoustic waves in the tank could attract the swimmers towards nodes of vibration.

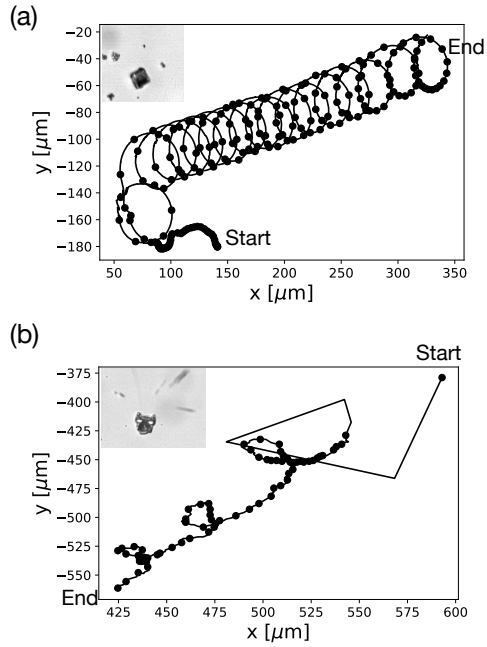

FIGURE 6 Trajectories of two swimmers exhibiting trochoid motions. (a) Trajectory of a swimmer under the influence of acoustic waves at 370 kHz and an amplitude of 50 mVpp. As shown in the picture, the bubble of the swimmer is orientated towards the substrate. (b) Trajectory of a swimmer under the influence of acoustic waves at 250 kHz and an amplitude of 160 mVpp. The swimmer is on the side, the bubble jet being lateral. The propulsion is visibly influenced by the acoustic streaming.

5 | CONCLUSION AND PERSPECTIVES

We have shown a new type of micro-swimmers that uses two different acoustic forces to navigate, namely the acoustic streaming force and the radiation force. The streaming force causes the swimmer to hover, thus overcoming adhesion forces, while the radiation force applies a lateral force to the swimmer to induce motion. These swimmers also exhibit ultra fast motion (velocity up to 0.35 m/s) but their velocity is tunable, and their motion direction can be controlled at smaller velocities. To tune the motion of the swimmer, we provide three simple control parameters, which are: the frequency, and the amplitude of the acoustic wave, and the orientation of the transducer. To compare the velocity and motion of the swimmers between different trials we focus on the maximal velocity. A more quantitative investigation of the micro-swimmers motion showed two regimes: one when the swimmers are moving along a straight line, and one when they make loops. Such difference in the motion behavior is due to the streaming force orientation. By using two transducers orientated perpendicularly to each other, we were able to induce a motion of the swimmer in two different directions. Similarly to Ahmed *et al.*,[32] another way to control the swimmer direction would be by having bubbles of different diameters on each side of the swimmer. Thus, by applying acoustic waves at different frequencies we could activate only one of the bubbles, subsequently inducing motion in a specific direction. Preliminary experiments have been conducted, but the resonance frequency of our bubbles are too close to allow such motion.

6 | SET-UP AND METHODS

6.1 | Fabrication of the microswimmers, and surface treatment

The 3D microobjects are fabricated using a two-photon polymerization setup (TEEM Photonics). The precision is of the order of the Nd:YAG microchip laser wavelength, 532 nm. The setup is mounted on the epifluorescence port of an inverted microscope. Fabrication parameters are described in detail in Liao et al. [33]. The micro-swimmers are designed on FreeCAD and fabricated on a glass cover slip (approximately 90 min per swimmer) in the shape of a hollow cube of size 20 μm with feet of height 6 μm, and an opening pointing downwards (size of the swimmer: 20×20×26 μm, size of the cavity: internal radius 7 μm, aperture radius 4 μm, see schematic in Fig. 7(a)). The solid micro-swimmer is surrounded by liquid polymer which is ultimately washed away with acetone in a CO_2 supercritical point dryer (Tousimis, model Autosamdri®-931). This device allows to reach the triple point and to rinse and dry the objects from the liquid polymer without putting much stress on it and thus preventing any collapse of the structure. The process generates 0.5 μm thick shells, creating hollow objects that can be reinforced inside with plates or bars. The material used is OrmoComp©, which is biocompatible but not biodegradable. Micro-swimmers can be observed using scanning electron microscopy (SEM) after fabrication. A typical image is shown on Fig. 7(a). Once they are fabricated, to make them hydrophobic we perform a silanization step using Trichloro(1H, 1H, 2H, 2H-perfluorooctyl) silane in its vaporous phase during 30 minutes. To prevent any future adhesion problems between the micro-swimmers and the substrate, the cover slip was previously treated using a technique described in **varma2016**. The idea is to grow a layer of a hydrophilic polymer brush of a micrometer thickness, preventing the silane to bond, and thus allowing to have a hydrophobic micro-swimmer on top of a hydrophilic surface.

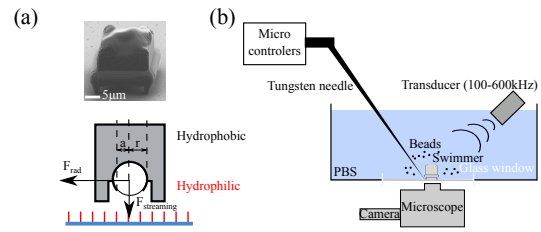

FIGURE 7 (a) AFM picture of a microswimmer and schematic of the silanized swimmer on top of the polymer brush. The swimmer in black is hydrophobic, while the polymer brush in red is hydrophilic. The dimensions of the swimmer are: 20×20×26 μm, and the cavity inside: internal radius: $r = 7\,\mu$m, aperture radius: $a = 4\,\mu$m. (b) Experimental set-up.

Once the micro-swimmers are fabricated, we want to study their motion. To do so, we use an original set-up described below.

6.2 | Experimental set-up

The experimental set-up consists of a three-liter tank made of Plexiglas with a rectangular glass window on the bottom (134 mm $\times$ 45 mm) filled with a 25-wt % PBS-water solution. The PBS-water solution is used to increase the bubble life time compared to regular water.[28] The tank is put on a microplatform that allows planar motion, mounted on top of an IX73 Olympus inverted microscope with 40$\times$ lenses (see Fig. 7(b)). This microscope is connected to a Phantom v2511 high-speed camera, with frame rates up to 20 000 frames per second. To generate acoustic waves, two different contact-less Ultran transducer (model GS350-D25-P50, centered at 325 kHz, focused; model GS200-D25-P50, centered at 183 kHz, focused) connected to an amplifier (Amplifier Research, model 75A250A, 75 watts, 10 kHz-250 MHz) are immersed at a distance of 10 cm from the microswimmer, corresponding to their focus length. Their broadband emissions allow to apply different frequencies to the swimmers to investigate their motion responses, so that an eventual resonance frequency could be found.

6.3 | Method

For the sake of reproducibility, at the beginning of each set of experiment, we put a bead of diameter 3.7 mm glued on a cover slip at the focus point of the microscope in the tank. Using a pulser/receiver (Panametrics-NDT, model 5073PR) we orient the transducer to reach the maximal signal amplitude. The second step is to place the microswimmer at the desired location and to tape (Duct tape©) the cover slip to the tank. A few milliliters of a solution containing 2 μm spherical particles is injected to observe the streamlines under the acoustic waves. To detach accurately the swimmers, a tungsten needle (World Precision Instruments, 50 mm long) connected to motorized actuators (Thorlabs, Z625B and Z725B) is used. Once the desired swimmer is detached, the acoustic waves can be generated.

REFERENCES

[1] S. Nain, N. Sharma, *Frontiers in Life Science* **2015**, *8*, 2–17.

[2] G. Iddan, G. Merron, A. Glukhovsky, P. Swain, *Nature* **2000**, *405*, 417.

[3] M. F. Hawthorne, J. I. Zink, J. M. Skelton, M. J. Bayer, C. Liu, E. Livshits, R. Baer, D. Neuhauser, *Science* **2004**, *303*, 1849–1851.

[4] L. E. Becker, S. A. Koehler, H. A. Stone, *Journal of Fluid Mechanics* **2003**, *490*, 15–35.

[5] J. E. Avron, O. Gat, O. Kenneth, *Phys. Rev. Lett.* **Oct. 2004**, *93*, 186001.

[6] W. Gao, X. Feng, A. Pei, C. R. Kane, R. Tam, C. Hennessy, J. Wang, *Nano Letters* **2014**, *14*, 305–310.

[7] W. F. Paxton, K. C. Kistler, C. C. Olmeda, A. Sen, S. K. St. Angelo, Y. Cao, T. E. Mallouk, P. E. Lammert, V. H. Crespi, *Journal of the American Chemical Society* **2004**, *126*, 13424–13431.

[8] W. F. Paxton, A. Sen, T. E. Mallouk, *Chemistry - A European Journal* **2005**, *11*, 6462–6470.

[9] S. Fournier-Bidoz, A. C. Arsenault, I. Manners, G. A. Ozin, *Chem. Commun.* **2005**, DOI 10.1039/B414896G.

[10] J. Vicario, R. Eelkema, W. R. Browne, A. Meetsma, R. M. La Crois, B. L. Feringa, *Chem. Commun.* **2005**, DOI 10.1039/B505092H.

[11] N. Mano, A. Heller, *Journal of the American Chemical Society* **2005**, *127*, 11574–11575.

[12] G. A. Ozin, I. Manners, S. Fournier-Bidoz, A. Arsenault, *Advanced Materials* **2005**, *17*, 3011–3018.

[13] R. Golestanian, T. B. Liverpool, A. Ajdari, *New Journal of Physics* **2007**, *9*, 126.

[14] I. Buttinoni, G. Volpe, F. Kaoemmel, G. Volpe, C. Bechinger, *Journal of Physics: Condensed Matter* **2012**, *24*, 284129.

[15] L. Zhang, L. Abbott, J. J.; Dong, K. E. Peyer, B. E. Kratochvil, H. Zhang, C. Bergeles, B. J. Nelson, *Nano Lett.* **2009**, *9*, 3663–3667.

[16] A. Ghosh, P. Fischer, *Nano Lett.* **2009**, *9*, 2243–2245.

[17] S. Tottori, L. Zhang, F. Qiu, K. K. Krawczyk, A. Franco-Obregon, B. J. Nelson, *Adv. Mater* **2012**, *24*, 811–816.

[18] W. Gao, S. Sattayasamitsathit, K. M. Manesh, D. Weihs, J. Wang, *J. Am. Chem. Soc.* **2010**, *132*, 14403–14405.

[19] R. Dreyfus, J. Baudry, M. L. Roper, M. Fermigier, J. Stone, H. A.; Bibette, *Nature* **2005**, *437*, 862–865.

[20] P. Fischer, A. Ghosh, *Nanoscale* **2011**, *3*, 557–563.

[21] J. G. Gibbs, Y. P. Zhao, *Appl. Phys. Lett.* **2009**, *94*, 163104–3.

[22] A. A. Solovev, Y. Mei, E. Bermu dez Urena, G. Huang, O. G. Schmidt, *Small* **2009**, *5*, 1688–1692.

[23] D. Ahmed, T. Baasch, B. Jang, S. Pane, J. Dual, B. J. Nelson, *Nano Letters* **2016**, *16*, 4968–4974.

[24] M. Kaynak, A. Ozcelik, A. Nourhani, P. E. Lammert, V. H. Crespi, T. J. Huang, *Lab Chip* **2017**, *17*, 395–400.

[25] W. Wang, L. A. Castro, M. Hoyos, T. E. Mallouk, *ACS Nano* **2012**, *6*, 6122–6132.

[26] J. Feng, J. Yuan, S. K. Cho, *Lab Chip* **2015**, *15*, 1554–1562.

[27] J. Feng, J. Yuan, S. K. Cho, *Lab Chip* **2016**, *16*, 2317–2325.

[28] N. Bertin, T. A. Spelman, O. Stephan, L. Gredy, M. Bouriau, E. Lauga, P. Marmottant, *Phys. Rev. Applied* **Dec. 2015**, *4*, 064012.

[29] T. G. Leighton, *Journal of Fluid Mechanics* **1994**, *272*, 407–408.

[30] T. Combriat, *http://www-liphy.ujf-grenoble.fr/Thomas-Combriat-en*.

[31] D. Allan, T. Caswell, N. Keim, C. van der Wel, trackpy: Trackpy v0.3.2, **Aug. 2016**.

[32] D. Ahmed, L. Mengqian, A. Nourhani, P. E. Lammert, Z. Stratton, H. Muddana, V. H. Crespi, T. J. Huang, *Scientific Reports* **2015**, *5*, 9744.

[33] C. Liao, M. Bouriau, P. L. Baldeck, J. Leon, C. Masclet, T. Chung, *Applied Physics Letters* **2007**, *91*, 033108.

ACKNOWLEDGEMENTS

Many thanks go to Lionel Bureau and Laetitia Gredy-Vurth for their help in the preparation of the polymer brushes, to Bahram Houchmandzadeh for fruitful conversations, and to Thomas Combriat for his help through out the project.